A subsurface pathway for salinity anomalies propagating from the northwestern subtropical Pacific to the eastern Luzon Strait

Youfang Yan[1], Eric P. Chassignet[2], Yiquan Qi[1], Zhichun Zhang[1], Kai Yu[3], Lingling Liu[4]

[1] State Key Laboratory of Tropical Oceanography (South China Sea Institute of Oceanology, Chinese Academy of Sciences), Guangzhou, China

[2] Center for Ocean-Atmospheric Prediction Studies, Florida State University, Tallahassee, Florida

[3] Oceanic Modeling and Observation Laboratory, Marine Science College, Nanjing University of Information Science and Technology, Nanjing, China

[4] Key Laboratory of Ocean Circulation and Waves, Institute of Oceanology, Chinese Academy of Sciences, Qingdao, China

Abstract

The subsurface ocean signal propagation from subtropics to tropics has been shown to play a vital role in low-frequency climate variability. In this study, monthly gridded temperature, salinity, and velocity datasets based on Argo profiles, long-term repeat hydrographic observations along 137°E section, and the regional ocean modeling system for 2003-2012 are used to investigate the subduction and propagation of subsurface salinity anomalies along 24.5-25.4kg.m^{-3} isopycnals in the northwestern Pacific. Both observational and modeling results suggest that the surface salinity anomalies in the northwestern subtropical Pacific (28-35°N, 140-160°E) could be subducted and advected to the eastern Luzon Strait via southwestward thermocline flows. In contrast to salinity anomalies generated in the northeastern subtropical Pacific that propagate slowly and dissipate strongly, these northwestern subtropical Pacific anomalies have a noticeable signature along their propagation pathway and arrive more quickly at the eastern Luzon Strait on time scales of 1-3 years.

1. Introduction

According to the ventilated thermocline theory (Luyten et al. 1983; Woods 1985), surface waters in the mid latitudes could be subducted and transported to the low latitudes via westward and equatorward gyre circulations. Using historical observations, Deser et al. (1996) demonstrated that temperature anomalies in the northeastern subtropical Pacific (NESP) can be subducted and advected equatorward to the tropics along isopycnals. By performing a trajectory analysis of waters in an oceanic general circulation model, Gu and Philander (1997) proposed three main pathways for the transport of subtropical waters to the low latitudes: 1) through a zigzag window, waters subducted in the NESP flow equatorward along isopycnals; 2) waters in the central/eastern SP subduct and move westward to the western boundary where they bifurcate, with some of the waters flowing to the tropics through an equatorward western boundary current (WBC); and 3) waters head northward back to the mid latitudes via the poleward WBC, generally taking ~10 years to reach the equator and western boundary and playing an important role in low-frequency climate variability.

Salinity (S), as a key physical parameter determining density of seawater (σ_θ) especially at mid and high latitudes and as an important marker of ocean circulation and air-sea freshwater, can modulate not only thermal variability but also the hydrologic cycle (e.g., Lukas 2001; Maes et al. 2005; Lagerloef et al. 2010). However, because of the general paucity of salinity observations, especially in the subsurface ocean, few studies have focused on the propagation of salinity in the mid and low latitudes. Taking advantage of recent Argo observations, several studies have investigated the interannual variability of subsurface salinity in the North Pacific (e.g., Sasaki et al. 2010; Ren and Riser 2010; Li et al. 2012a; Yan et al. 2012). Among others, Sasaki et al (2010) reported that anomalous spiciness (potential temperature and salinity variation on isopycnals) generated in the NESP can propagate southwestward to the equator. However, because of the strong dissipation, these anomalies could not reach the western boundary. Using Argo observations, Li et al

(2012a) and Kolodziejczyk and Gaillard (2012) found a remarkably strong attenuation of spiciness in the NESP along its propagation route, consistent with the results of Sasaki et al. (2010). Alternatively, instead of studying upstream anomalies in the NESP, Yan et al. (2012; 2013) investigated the downstream subsurface salinity anomalies in the eastern Luzon Strait (ELS). They found the anomalies in the ELS are not directly traced back to those in the NESP; instead, they are apparently related to those in the northwestern subtropical Pacific (NWSP).

Although the possible connection of the subsurface salinity anomaly between the ELS and the NWSP has been investigated by Yan et al. (2012; 2013), the detailed characterization of this anomaly and its propagation pathway are still not clear. How fast does this anomaly propagate? Does it extend to the low latitude regions? These questions will be addressed in the present study. The remainder of the paper is organized as follows: A brief description of the data and method of analysis are presented in section 2; the subduction and propagation pathways of salinity anomalies in the northwestern Pacific are explained in section 3; and results are summarized and discussed in section 4.

2. Data and method of analysis

The monthly mean 1°×1° temperature and salinity fields compiled by Hosoda et al. (2008), known as the Grid Point Values of the Monthly Objective Analysis (MOAA GPV) based mainly on Argo observations for the period 2003-2012, are used in this study. In situ measurements by conductivity-temperature depth along 137°E sections provided by the Japan Meteorological Agency (JMA) are also used. In order to study salinity propagation pathways, 2003-2012 velocity model outputs were used from the Regional Ocean Modeling System (ROMS) with 1/8º horizontal resolution from 45°S to 65°N and from 99°E to 70°W, and 30 levels in the vertical. For a detailed description and validation of ROMS with in situ observations, the reader is referred to Zhang et al. (2015, personal communication). The evaporation (E) from the Objectively Analyzed air-sea Fluxes (OAFlux) project was provided by the Woods Hole Oceanographic Institution (Yu and Weller 2007) while the precipitation (P) fields come from the Global Precipitation Climatology Project (GPCP). Finally, wind stresses from the Cross-Calibrated Multi-Platform (CCMP) are used, as are sea surface geostrophic velocity anomalies provided by Archiving, Validation and Interpretation of Satellite Oceanographic (AVISO) on a 0.25°×0.25°.

The Montgomery geostrophic streamfunction ψ (Montgomery 1937) is defined by

$$\psi = (\mathrm{P} - \mathrm{P}_0)\hat{\delta} - \int_{P_0}^{P} \hat{\delta}(\mathrm{S}[\mathrm{p}'], \theta[\mathrm{p}'], \mathrm{p}')\,\mathrm{dP}' \qquad (1)$$

Where P is the reference pressure, P_0 is the sea surface pressure, $\hat{\delta}$ is the specific volume anomaly. The mean surface geostrophic velocities are derived from the MDT_CNES-CLS09 product (Rio et al. 2011). The statistical analysis of interannual salinity patterns on the given isopycnal surface is performed with the Extended Empirical Orthogonal Function (EEOF). Compared to the classical EOF analysis, the EEOF analysis can catch the propagating pattern by introducing time lag into the covariance matrix. The annual subduction rate R_{ann}, which is calculated by tracing water parcels released at the base of the winter mixed layer for one year in a Lagrangian framework, is expressed as (Huang and Qiu 1998):

$$R_{ann} = -\frac{1}{T}\int_{t_1}^{t_2} w_{mb}\,dt - \frac{1}{T}[h_{\mathrm{m}}(t_2) - h_{\mathrm{m}}(t_1)], \qquad (2)$$

where T represents the time period of integration; t_1 and t_2 are the end of the first and second winter, respectively; h_m is the winter mixed layer depth (MLD); and w_{mb} is the vertical velocity at the base of the mixed layer.

3. Isopycnal salinity anomalies and their propagation in the northwestern subtropical Pacific (NWSP)

3.1 Salinity anomalies

The recent availability of Argo observations has led to the study of isopycnal salinity anomalies in the NWSP (Li et al. 2012a; Yan et al. 2012; 2013; Sugimoto et al. 2013). Because maximum subduction occurs in the winter, we first show in Fig.1b the standard deviation of winter salinity anomalies averaged on the 24.5-25.4kg.m^{-3} isopycnals, where the water exhibits a sustained freshening trend (Yan et al. 2012; 2013; Nan et al. 2015). There is a band of large salinity variability in the Kuroshio Extension, with magnitude up to 0.1 PSU. This anomaly compares favorably with that of Yan et al. (2013) and Nan et al. (2015), and spreads along the 24.5-25.4kg.m^{-3} outcrop lines (Fig.1c).

The salinity distribution is generally the result of a balance between surface freshwater fluxes (precipitation P, evaporation E) and ocean dynamics. As shown in Fig. 1a, the standard deviation of E-P attains its maximum at the northern rims of subtropical gyre (35°N), located slightly northwestward of the area of maximum salinity variability, most notably in the southeastern side of study region. This displacement suggests the potential impact of ocean dynamics on salinity variability. A careful examination of surface wind stress indicates that a strong northwesterly wind prevails in the maximum variability of the E-P region (Fig. 1a). The northwesterly wind drives a positive salinity advection toward the salinity maximum variability region, thus leading to a southeastward shift of salinity maximum to the region of maximum E-P variability. In addition, the maximum salinity variability is found in the regions where the vertical Ekman pumping is predominantly downward (Fig.1a). The downward Ekman pumping provides a favorable condition for the subduction of high-variability surface waters into the ocean interior, although the lateral induction becomes dominant as a result of large winter mixed layer depth (MLD) gradients (Fig. 1c) in the studied region (Suga et al. 2008).

By transferring the waters from the mixed layer into the ocean interior, subduction is another kinematical and dynamical process coupling the atmosphere and the subsurface ocean. Before proceeding to calculate the subduction rate in the NWSP, we first examine the MLD. As shown in Fig. 1c, the winter MLD is generally shallow (~50 m) in the low latitudes and gradually becomes deeper toward the higher latitudes, with a maximum lying around the southern edge of maximum salinity variability. This maximum MLD allows winter mixed layer waters to subduct into the thermocline (Qiu and Huang 1995). The annual subduction rate, which is calculated using the Argo temperature and salinity data combined with the NCEP wind field, is shown in Fig.1d. It is worth noting that the regions of largest annual subduction rate have been found to be at the southern edge of the highest salinity variability and maximum MLD region (Fig.1b, 1c and 1d), reflecting the dominant contribution of lateral induction in the salinity subduction, consistent with Qiu and Huang (1995) and Suga et al. (2008).

To demonstrate the horizontal transport of the subducted salinity anomalies in the thermocline, we release passive particles at the base of the mixed layer in February and advect them with the flow field for one year. The trajectories of the passive particles (Fig. 1d) match well with the streamlines of Montgomery geostrophic flow on 24.5-25.4 kg.m^{-3} isopycnals, suggesting the subducted salinity anomalies in the outcropping regions (Fig.1e-1f) may be transferred to the western tropical Pacific by a southwestward horizontal flow.

3.2 Propagation pathway

To illustrate where and when the salinity anomalies propagate, the EEOF decomposition from a statistical perspective is first applied with time lags of 1, 3, 5, 7, 9, 11, and 13 months, respectively. The spatial pattern of the first mode (EEOF1), with time lags of 1 month and accounting for ~70.1% of the total variance and explaining a significant part of salinity variability, and the corresponding time coefficients are illustrated in Fig. 2a and 2b. The first mode shows a marked freshening of waters in the NWSP with salinity decreasing during 2003-12, consistent with the results of Fig.1e-1f and those of Sugimoto et al. (2013) and Nan et al. (2015). The strongest freshening trend occurs in the surface layer (-0.2psu/10yr) near 30°N and decreases against depth. It should also be noted that the salinity anomalies south of 15°N are entirely out of phase with those north of 15°N, displaying a dipolar structure. This dipolar structure is also found in the trends of salinity anomalies based on Argo observations and the repeated oceanographic observation section along 137°E (Fig. 3). The dissimilar trends in the north and south of 15°N indicate that the mechanisms controlling the salinity in these two regions are quite different. The reason for this difference is unclear and is beyond the scope of this study. To illustrate the propagation pathway of salinity anomalies north of 15°N, the contour lines of -0.15 PSU with time lags of 1, 3, 5, 7, 9, 11, and 13 months based on EEOF are shown (Fig. 2a). We observe that a negative anomaly emerges and propagates southwestward from the region south of the Kuroshio Extension toward the western boundary, taking about 13 months to reach the ELS (see the label number of contours). This propagation time is consistent with the results of Oka [2009], Oka and Qiu [2012] and Qiu and Chen [2013]. Consistent with the results of Nan et al. (2015), the southwestward propagation of the signal corresponds well with the Pacific Decadal Oscillation (PDO) ($r=-0.68$), which is significantly different from zero at the 95% confidence level ($r=-0.596$) according to a Student's t test. Compared to the PDO index, the correlation ($r=-0.60$) between the anomalies and the Nino3.4 index is lower and possibly insignificant during 2003-2012.

To further document the propagation pathway, we now focus on the latitude-time diagram of salinity anomalies averaged vertically over the 24.5-25.4kg.m^{-3} isopycnals along the Montgomery geostrophic streamlines between 28.0 and 29.0m^2/s^2 (Fig. 2d). The latitude-time diagram of salinity anomalies indicates that the propagated salinity signals exhibit decadal timescale variability and experience two major phase-flipping events in 2005 and 2009. In order to determine what causes these subsurface salinity changes, we look at the surface salinity anomalies averaged over the subduction region (28°-35°N, 140°-160°E). Two extreme opposing phases of the surface salinity anomalies are found in 2004-2006 and 2009-2011, consistent with the mixed layer salinity variability in the subtropical mode water formation region (Sugimoto et al. 2013). The timing of these peaks nearly coincides with that of the subsurface salinity anomalies, suggesting that the propagation of salinity anomalies along the isopycnals mainly comes from the surface in the outcrop zones.

To view the full cycle of salinity anomalies propagation in the NWSP, in Fig. 4 we plot the monthly maps of positive salinity anomalies averaged over 24.5-25.4kg.m^{-3} isopycnals during 2005-2006, corresponding to the strongest salinity anomalies as shown in Fig. 2d. This reveals that the anomaly is first detected at 25°-35°N in Feb 2005 (Fig. 3a); it then migrates southwestward along the contours of the Montgomery geostrophic streamfunction and approaches the ELS in Jan 2006 (Fig. 3l). The path of this anomaly is consistent with the results of EEOF (Fig. 2a), suggesting that the surface salinity anomalies in the northwest subtropical outcropping region may propagate to the ELS via the southwestward subtropical gyre circulations.

Previous studies (Parr 1938; Montgomery 1938) have demonstrated that salinity is also a useful dynamical tracer conservatively following parcels' trajectory along isopycnal surfaces. Thus, here we performed forward Lagrangian particle tracing experiments based on every three days velocity of ROMS for 2003-2012 in order to independently identify the propagation path of the subsurface salinity anomalies in the subtropical gyre. The trajectories of these particles are shown in Fig. 5. All the particles can be traced to the ELS by southward subtropical gyre circulations, with tracing periods ranging from 1-3 years. The particles released in the western higher salinity trend subduction areas (see Fig. 3a) can be traced to the ELS faster (~1yr) than those released in the lower salinity trend eastern areas (~3yrs). In addition, the tracing period is not qualitatively sensitive to positive or negative salinity anomalies (Fig. 5b and Fig. 5c), which suggests that salinity variations in the ELS can be influenced by upstream salinity variations through southwestward subtropical gyre circulations.

4. Summary and discussion

This study provides a detailed description of the subduction and propagation of subsurface salinity anomalies in the northwest Pacific using the temperature, salinity, and velocity data provided mainly by Argo observations, in situ observations, and ROMS. Tracing of the subsurface salinity anomalies was accomplished by conducting an EEOF analysis, examining the extreme salinity anomalies along 24.5-25.4kg.m^{-3} isopycnals, and eventually designing forward Lagrangian particle tracing experiments. As a result, we found that salinity anomalies generated in the northwest Pacific subduction region (28°-35°N, 140°-160°E) can be subducted and can propagate to the ELS via southwestward subtropical gyre circulations on time scales of 1 to 3years.

The possible connection between the mid latitudes and the western boundary via the subsurface salinity propagation in the North Pacific has been recently examined; however because of strong dissipation, the salinity anomalies originating in the NESP nearly vanished before reaching the western boundary (e.g., Li et al. 2012b; Kolodziejczyk and Gaillard 2012). In this study, we show that the anomalies generated in the NWSP outcropping region (28°-35°N, 140°-160°E) are strong and they reach the ELS on time scales of 1 to 3 years.

Although the propagation pathway and timing of salinity anomalies between the mid latitudes and the ELS is addressed in this study, several open questions still remain. What mechanism controls the generation and subduction of salinity anomalies in the outcrop region? How do the salinity anomalies affect its downstream western Pacific warm pool change? A recent study has suggested that the warm pool change is related not only to the large-scale air-sea processes, but also to the subsurface ocean processes (Qu et al. 2013). Knowledge of the subsurface salinity change and its linkage with the warm pool's thermocline structure would provide a crucial basis for understanding of ocean-atmosphere interaction and the climate effects of subducted salinity anomalies.

Acknowledgments

This study was supported by the National Basic Research Program of China (2013CB430301), the Strategic Priority Research Program of the Chinese Academy of Sciences (XDA11010203), and the National Natural Science Foundation of China (41276025).

References

Deser, C., M. A. Alexander, and M. S. Timlin, 1996: Upper-ocean thermal variations in the North Pacific during 1970-1991, *J. Clim*., 9, 1840-1855.

Gu, D., and G. S. Philander, 1997: Interdecadal climate fluctuations that depend on exchanges between the tropics and extratropics, *Science*, 275, 805-807.

Hosoda, S., T. Ohira, and T. Nakamura, 2008: A monthly mean dataset of global oceanic temperature and salinity derived from Argo float observations, *JAMSTEC Report of Research and Development*, 8, 47-59.

Huang, R. X., and B. Qiu, 1998: The structure of the wind-driven circulation in the subtropical South Pacific Ocean, *J. Phys. Oceanogr*., 28, 1173-1186.

Huang, B., and Z. Liu, 1999: Pacific subtropical-tropical thermocline water exchange in the National Centers for Environmental Prediction ocean model, *J. Geophys. Res*., 104, 11065-11076.

Kolodziejczyk, N., and F. Gaillard, 2012: Observation of spiciness interannual variability in the Pacific pycnocline, *J. Geophys. Res*., 117, C12018, doi: 10.1029/2012JC008365.

Lagerloef, G., R. Schmitt, J. Schanze, and H. Y. Kao, 2010: The Ocean and the global water cycle, *Oceanography*, 23(4), 82-93.

Li, Y. L., F. Wang, and F. G. Zhai, 2012a: Interannual variations of subsurface spiciness in the Philippine Sea: Observations and mechanism, *J. Phys. Oceanogr*., 42, 1022-1038.

Li, Y., F. Wang, and Y. Sun, 2012b: Low-frequency spiciness variations in the tropical Pacific Ocean observed during 2003-2012, *Geophys. Res. Lett*., 39, L23601, doi: 10.1029/2012GL053971.

Luyten, J., J. Pedlosky, and H. M. Stommel, 1983: The ventilated thermocline, *J. Phys. Oceanogr*., 13, 292-309.

Lukas, R., 2001: Freshening of the upper thermocline in the North Pacific subtropical gyre associated with decadal changes of rainfall, *Geophys. Res. Lett*., 28, 3485-3488.

Maes, C., J. Picaut, and S. Belamari, 2005: Importance of the salinity barrier layer for the buildup of El Nino, *J. Clim*., 18, 104-118.

Montgomery, R. B., 1937: A suggested method for representing gradient flow in isentropic surfaces, *Bull. Amer. Meteor. Soc*. 18, 210-212.

Montgomery, R. B., 1938: Circulation in upper layers of southern North Altantic deduced with use of isentropic analysis, *Pap. Phys. Oceanogr*., 6, 1-55.

Nan, F., F. Yu, H. Xue, R. Wang, and G. Si, 2015: Ocean salinity changes in the northwest Pacific subtropical gyre: the quasi-decadal oscillation and the freshening trend, J. Geophys. Res.Oceans, 120, doi: 10.1002/2014JC010536.

Oka, E., 2009: Seasonal and interannual variation of North Pacific subtropical mode water in 2003-2006, *J. Oceanogr*., 65,151-164.

Oka, E., and B. Qiu, 2012: Progress of North Pacific mode water research in the past decade, *J. Oceanogr*., 68, 5-20.

Parr, A. E., 1938: Isopycnic analysis of current flow by means of identifying properties, *J. Mar. Res*., 1, 133-154.

Qiu, B., and R. X. Huang, 1995: Ventilation of the North Atlantic and North Pacific: Subduction versus obduction, *J. Phys. Oceanogr*., 25, 2374-2390.

Qiu, B., and S. Chen, 2013: Concurrent decadal mesoscale eddy modulations in the Western North Pacific subtropical Gyre, *J. Phys. Oceanogr*., 43, 344-358.

Qu, T. D, S. Gao, R. A. Fine, 2013: Subduction of South Pacific Tropical Water and Its Equatorward Pathways as Shown by a Simulated Passive Tracer, *J. Phys. Oceanogr*., 43, 1551-1565.

Ren, L., and S. C. Riser, 2010: Observations of decadal time scale salinity changes in the subtropical thermocline of the North Pacific Ocean, *Deep-Sea Research*, 57, 1161-1170.

Rio, M. H., S. Guinehut, and G. Larnicol, 2011: New CNES-CLS09 global mean dynamic topography computed from the combination of GRACE data, altimetry, and in situ measurements, *J. Geophys. Res*., 116, doi: 10.1029/2010JC006505.

Sasaki, Y. N., N. Schneider, N. Maximenko, and K. Lebedev, 2010: Observational evidence for propagation of decadal spiciness anomalies in the North Pacific, *Geophys. Res. Lett*., 37, L07708, doi: 07710.01029/02010GL042716.

Toshio Suga,Yoshikazu Aoki, Hiroko Saito, Kimio Hanawa, 2008:Ventilation of the North Pacific subtropical pycnocline and mode water formation, Progress in Oceanography, 77, 285-297.

Sugimoto, S., N. Takahashi, and K. Hanawa, 2013: Marked freshening of North Pacific subtropical mode water in 2009 and 2010: Influence of freshwater supply in the 2008 warm season, *Geophys. Res. Lett*., 40, 3102-3105.

Woods, J. D., 1985: Physics of thermocline ventilation, In Coupled Atmosphere-Ocean Models, ed. by J. C. J. Nihoul.

Yan, Y., D. Xu, Y. Qi, and Z. Gan, 2012: Observations of freshening in the northwest Pacific subtropical Gyre near Luzon Strait, *Atmosphere-Ocean*, doi: 10.1080/07055900.07052 012.07715078.

Yan, Y., E. P. Chassignet, Y. Qi, and W. K. Dewar, 2013: Freshening of Subsurface Waters in the Northwest Pacific Subtropical Gyre: Observations and Dynamics, *J. Phys. Oceanogr*., 43, 2733-2750.

Yu, L., X. Jin, and R. A. Weller, 2008: Multidecade Global Flux Datasets from the Objectively Analyzed Air-sea Fluxes (OAFlux) Project: Latent and sensible heat fluxes, ocean evaporation, and related surface meteorological variables. Woods Hole Oceanographic Institution, OAFlux Project Technical Report. OA-2008-01, 64pp. Woods Hole. Massachuse.

Zhichun ZHANG, Huijie XUE, Fei Chai, Yi Chao, 2015: Inter-annual Variability of the North Equatorial Current Based on Model Results, Under Reviewed.

Figures

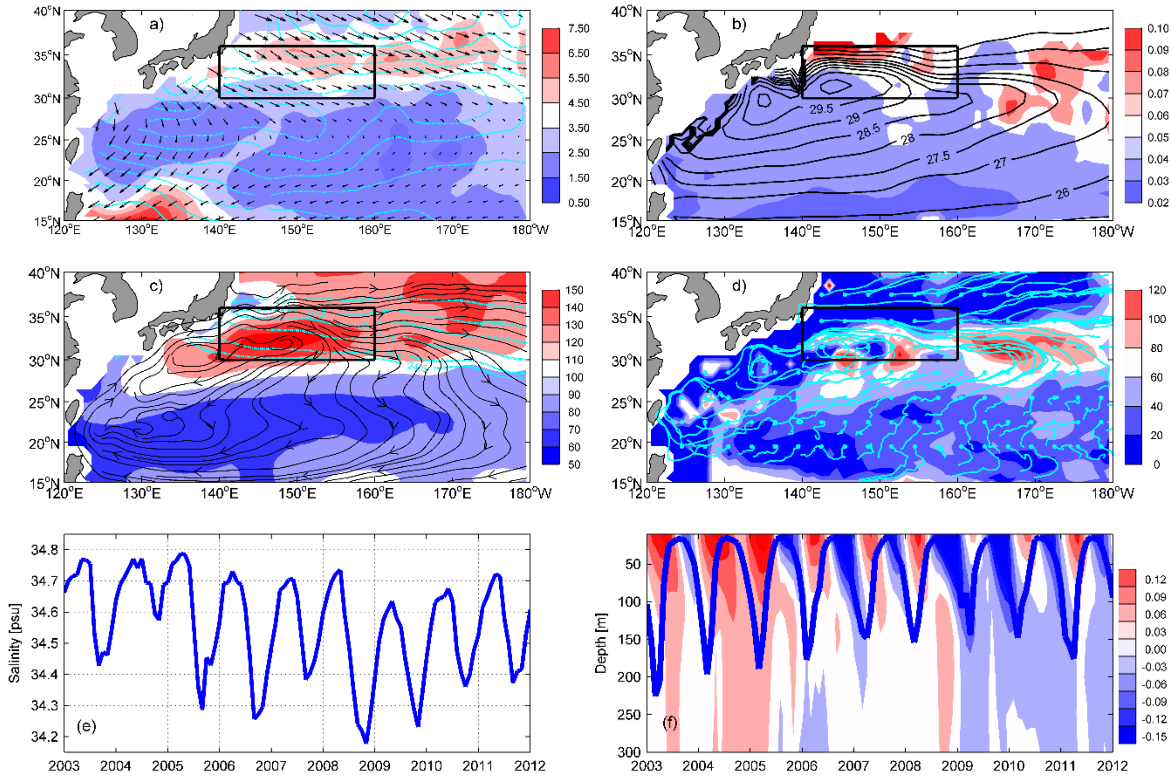

Fig.1: (a) Winter standard deviation (STD) of evaporation minus precipitation (E-P; cm/month) from OAflux and GPCP (shading) with surface wind stress (N.m^{-2}; black arrows) and its curl (N.m^{-3}; cyan contours: solid for positive value, dash for negative value) from CCMP during 2003-2012. (b) Winter STD of salinity anomalies on the 24.5-25.4 kg/m^3 isopycnals (shading) and contours of the mean Montgomery geostrophic streamfunction referred to 2000dbar (m2/s2; black contours) on the 24.5-25.4 kg/m^{3}isopycnals during 2003-2012. (c) Winter mixed layer depth (m; shading), which is defined as the depth at which density increases by 0.125kg.m^{-3} from the surface, with the 24.5-25.4 kg/m^3 isopycnal line (cyan contours) and sea surface geostrophic velocity streamlines (black arrows) from AVISO. (d) Annual mean subduction rate (m/year; shading) with Lagrangian trajectories (cyan curves) over a 1-year period based on the MOAA GPV data. Starting points are indicated by dots where particles are released from the base of the late winter (Feb) mixed layer. The along-isopycnal geostrophic velocities are calculated using the 2000-m depth as the reference level based on salinity and temperature of the MOAA GPV data. Here winter months are Dec-Feb. (e) Monthly time series of MLS averaged within the subduction region. (f) Vertical distribution of salinity anomalies (shading) and MLD (blue lines) within the subduction region. The black rectangular area indicates the subduction region (140°E-160°E, 28°N-35°N).

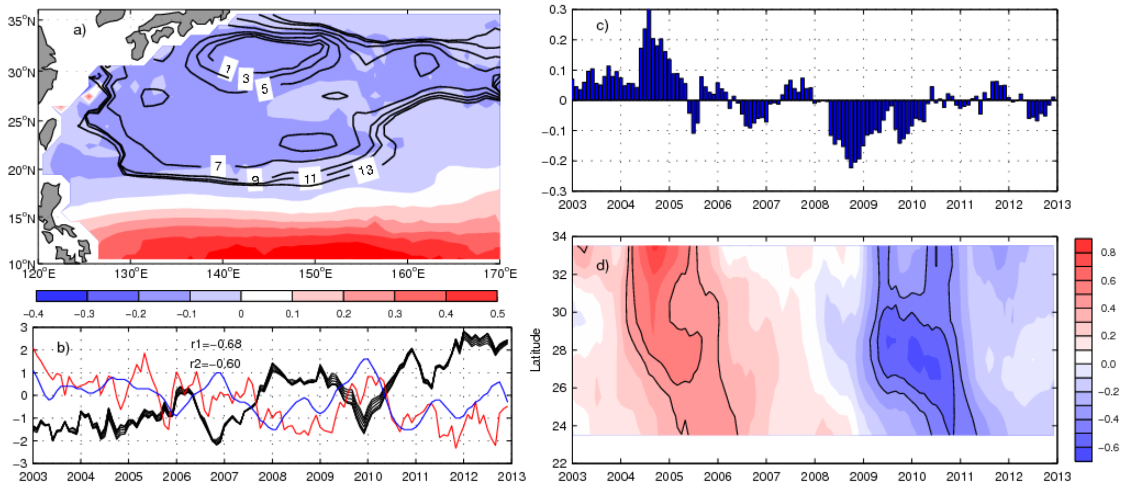

Fig.2: (a) The spatial patterns of the first extended empirical orthogonal function mode (EEOF1) of salinity anomalies (in 10×PSU) averaged over the 24.5-25.4kg/m^{3}isopycnals with time lags 1 months. The contours of -0.15 PSU with time lags 1, 3, 5, 7, 9, 11 and 13 months are highlighted for easy viewing (black curves). (b) The corresponding time coefficients of EEOF1 with time lags 1, 3, 5, 7, 9, 11 and 13 months (black lines), Nino3.4 index (blue line) and PDO index (red line); r1 and r2 is the correlation coefficient between the time coefficients of EEOF1 with time lags 1 month with PDO index and Nino3.4 index, respectively. (c) The surface salinity anomalies averaged over the outcropping region (140°E-160°E, 28°N-35°N). (d) Latitude-time diagram of salinity anomalies (in 10×PSU) averaged vertically over the 24.5-25.4kg/m^3 isopycnals along the Montgomery geostrophic streamlines between 28.0 and 29.0m^2/s^2. Contour interval is 0.1PSU, and contours of -0.5, -0.4, 0.4 and 0.5 PSU are marked as black curves.

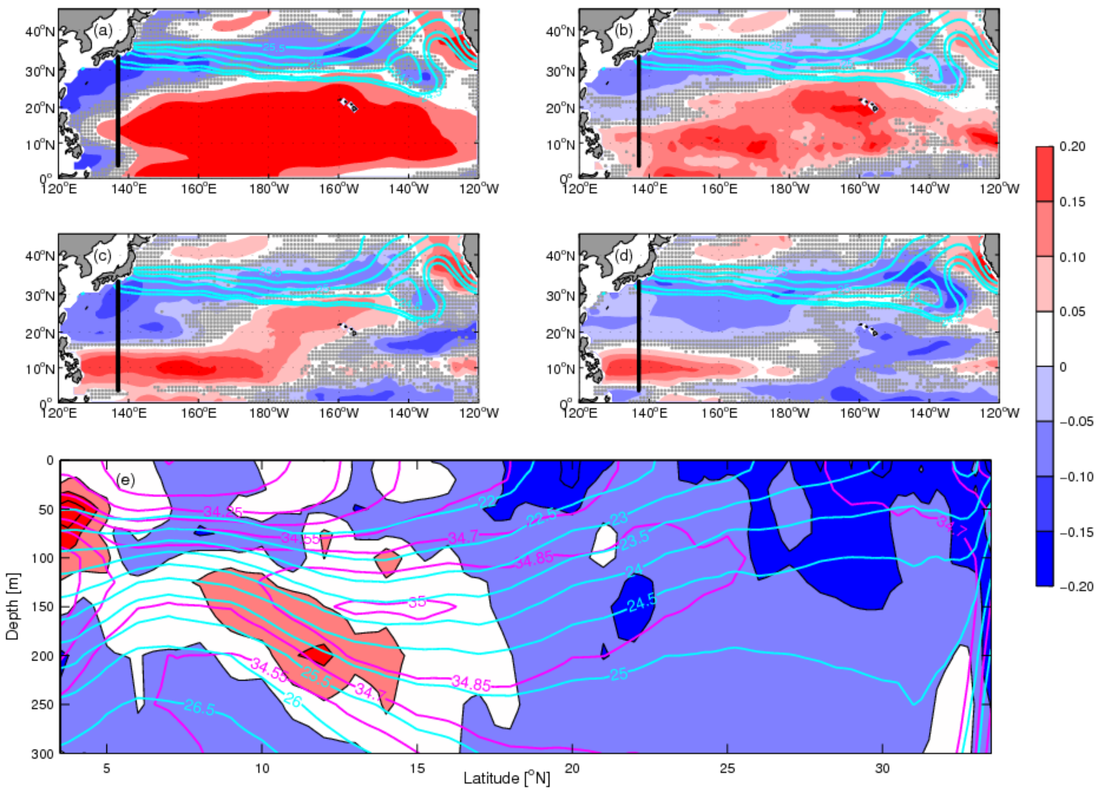

Fig.3: Linear trends [PSU/10yr] of salinity anomalies on (a) sea surface; (b) 23.5 kg/m^3; (c) 24.5 kg/m^3; (d) 25.4 kg/m^{3}over the period 2002-2013 based on monthly mean MOAA_ARGO data. (e) Linear trends [PSU/10yr] of salinity anomalies along the 137°E section based on the 137°E oceanographic data obtained by JMA research vessels over 2002-2013. The regions where the linear trends are not significant at the 95% confidence level are hatched in gray using Mann Kendall method. The locations of 137°E section are shown in black lines.

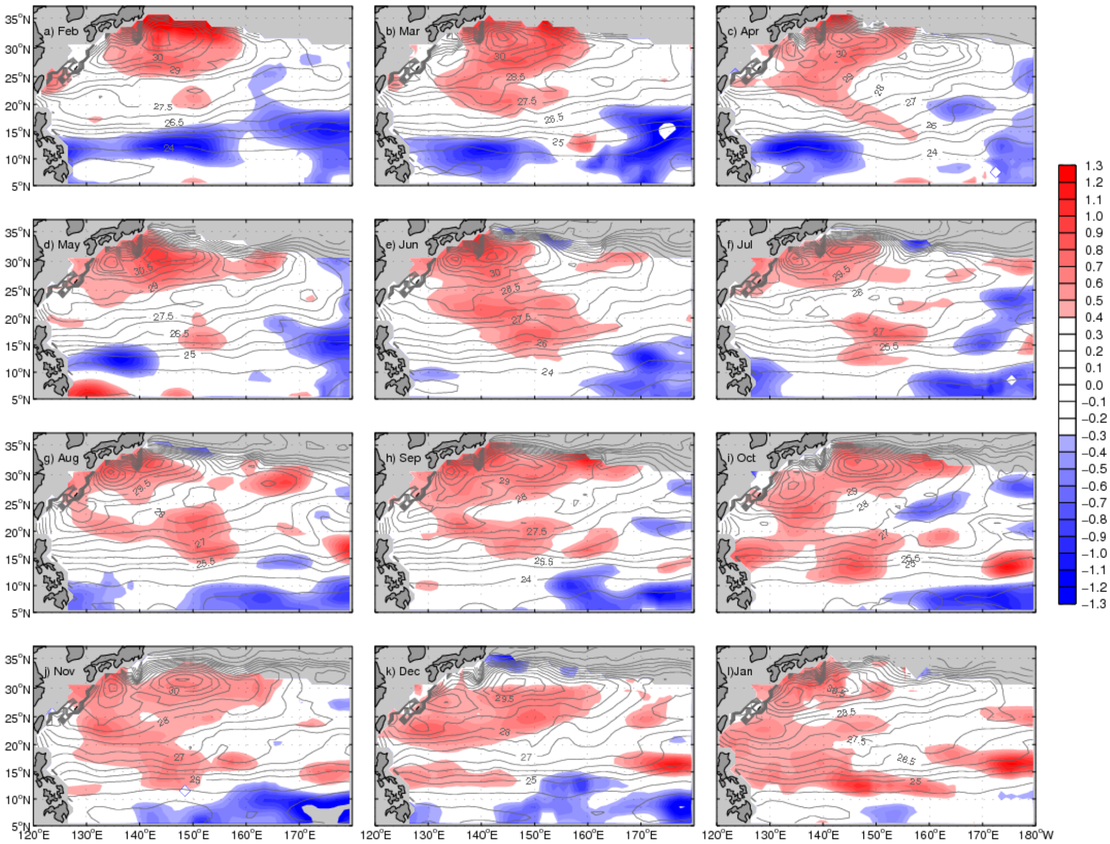

Fig.4: Monthly maps of salinity anomalies averaged over the 24.5-25.4 kg.m^{-3} isopycnals (shading in 10×PSU) and the corresponding contours of the Montgomery geostrophic streamfunction referred to 2000dbar for Feb 2005 to Jan 2006 (gray contours) based on the Argo observations.

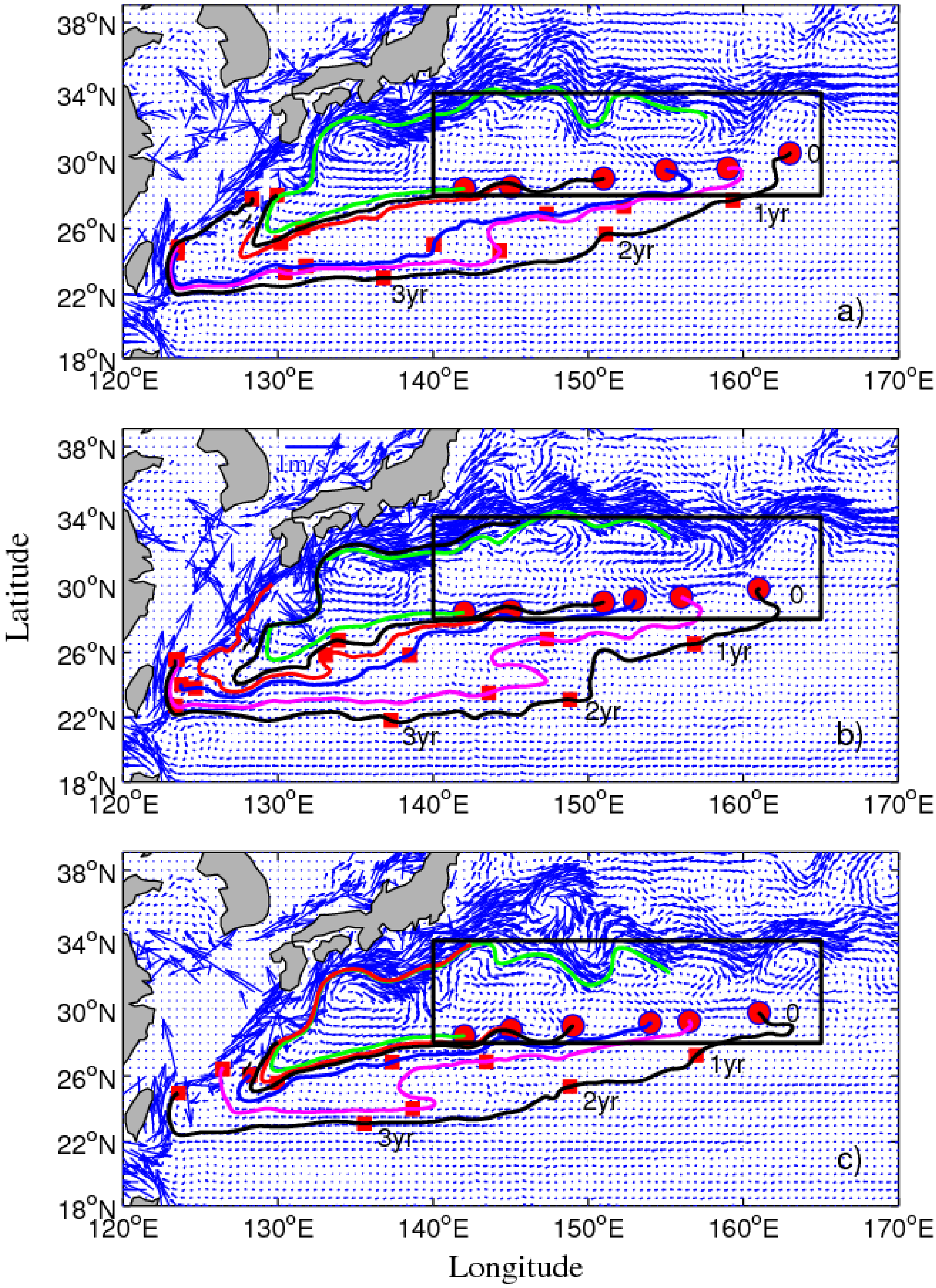

Fig.5: Trajectories of the forward Lagrangian particle tracing of the salinity anomaly signals based on the velocity mean vertically averaged between the potential density of 24.5 and 25.4 kg/m^3(vector; m/s) for a) 2003-2012; b) 2004-2006; c) 2009-2011. Red circles indicate the starting locations, the red rectangles indicate the positions of the signals propagate for one year, the black rectangular area indicates the subduction region (140°E-160°E, 28°N-35°N).